Check for updates

AGU ADVANCING EARTH AND SPACE SCIENCE

Geophysical Research Letters®

RESEARCH LETTER
10.1029/2022GL097953

The Chemistry of Mercury in the Stratosphere

Alfonso Saiz-Lopez[1], A. Ulises Acuña[1], Anoop S. Mahajan[2], Juan Z. Dávalos[1], Wuhu Feng[3,4], Daniel Roca-Sanjuán[5], Javier Carmona-García[1,5], Carlos A. Cuevas[1], Douglas E. Kinnison[6], Juan Carlos Gómez Martín[7], Joseph S. Francisco[8], and John M. C. Plane[3]

[1]Department of Atmospheric Chemistry and Climate, Institute of Physical Chemistry Rocasolano, CSIC, Madrid, Spain, [2]Centre for Climate Change Research, Indian Institute of Tropical Meteorology, Ministry of Earth Sciences, Pune, India, [3]School of Chemistry, University of Leeds, Leeds, UK, [4]NCAS, School of Earth and Environment, University of Leeds, Leeds, UK, [5]Institut de Ciència Molecular, Universitat de València, València, Spain, [6]Atmospheric Chemistry Observations and Modelling, NCAR, Boulder, CO, USA, [7]Instituto de Astrofísica de Andalucía, CSIC, Granada, Spain, [8]Department of Earth and Environmental Science and Department of Chemistry, University of Pennsylvania, Philadelphia, PA, USA

Key Points:

- A new chemical mechanism for photosensitized mercury oxidation is proposed
- Above the UV-absorbing ozone layer, elemental mercury is quickly oxidized by photosensitized reactions
- In the lower stratosphere, the photosensitized oxidation is replaced by much slower thermal oxidation driven by Cl, OH, and Br radicals

Supporting Information:

Supporting Information may be found in the online version of this article.

Correspondence to:

A. Saiz-Lopez and J. M. C. Plane,
a.saiz@csic.es;
J.M.C.Plane@leeds.ac.uk

Citation:

Saiz-Lopez, A., Acuña, A. U., Mahajan, A. S., Dávalos, J. Z., Feng, W., Roca-Sanjuán, D., et al. (2022). The chemistry of mercury in the stratosphere. *Geophysical Research Letters*, *49*, e2022GL097953. https://doi.org/10.1029/2022GL097953

Received 18 JAN 2022
Accepted 24 MAY 2022

Author Contributions:

Conceptualization: Alfonso Saiz-Lopez, A. Ulises Acuña, John M. C. Plane
Investigation: Alfonso Saiz-Lopez, A. Ulises Acuña, Anoop S. Mahajan, Juan Z. Dávalos, Daniel Roca-Sanjuán, Javier Carmona-García, Carlos A. Cuevas, Douglas E. Kinnison, Juan Carlos Gómez Martín, Joseph S. Francisco, John M. C. Plane
Methodology: Alfonso Saiz-Lopez, A. Ulises Acuña, Anoop S. Mahajan, Juan Z. Dávalos, Wuhu Feng, Daniel Roca-Sanjuán, Javier Carmona-García, Carlos A. Cuevas, Douglas E. Kinnison,

© 2022. The Authors.
This is an open access article under the terms of the Creative Commons Attribution-NonCommercial-NoDerivs License, which permits use and distribution in any medium, provided the original work is properly cited, the use is non-commercial and no modifications or adaptations are made.

Abstract Mercury, a global contaminant, enters the stratosphere through convective uplift, but its chemical cycling in the stratosphere is unknown. We report the first model of stratospheric mercury chemistry based on a novel photosensitized oxidation mechanism. We find two very distinct Hg chemical regimes in the stratosphere: in the upper stratosphere, above the ozone maximum concentration, Hg^0 oxidation is initiated by photosensitized reactions, followed by second-step chlorine chemistry. In the lower stratosphere, ground-state Hg^0 is oxidized by thermal reactions at much slower rates. This dichotomy arises due to the coincidence of the mercury absorption at 253.7 nm with the ozone Hartley band maximum at 254 nm. We also find that stratospheric Hg oxidation, controlled by chlorine and hydroxyl radicals, is much faster than previously assumed, but moderated by efficient photo-reduction of mercury compounds. Mercury lifetime shows a steep increase from hours in the upper-middle stratosphere to years in the lower stratosphere.

Plain Language Summary Mercury is a toxic pollutant that is released to the atmosphere as a result of human activities and from natural sources. Due to its long lifetime, mercury can travel around the world and also can be injected to the stratosphere via convective uplift in the tropical regions. Aircraft observations have reported significant concentrations of different forms of mercury in the stratosphere, however, the chemistry of mercury in this region of the atmosphere remains unexplored. This work reports a new chemical framework that sheds light on the chemical cycling of stratospheric mercury. The results reveal the stratosphere as a unique environment for mercury chemistry that has potential implications for the global transport of this metal.

1. Introduction

Mercury (Hg) is a neurotoxin with a long lifetime in the Earth system, which exchanges between the atmosphere, continents, and oceans (Driscoll et al., 2013; Lyman et al., 2020; Obrist et al., 2018). A large range of human activities result in emissions of mercury to the atmosphere, predominantly (80%–90%) as elemental mercury (Hg^0) (AMAP/UN, 2019; Gustin et al., 2015), characterized by a low chemical reactivity. Atmospheric mercury deposits to ecosystems after oxidation to form water-soluble $Hg^{I,II}$ species (Horowitz et al., 2017) as well as in elemental form (Jiskra et al., 2021). Therefore, understanding the atmospheric mercury cycling between Hg^0 and oxidized monovalent Hg^I and divalent Hg^{II} forms is key for accurate assessments of its global transport and input into ecosystems via surface deposition. In current mechanistic and modeling research it is assumed that only highly reactive bromine atoms (Br) or radicals (OH) can initiate the oxidative chain of gas-phase ambient mercury (Horowitz et al., 2017; Hynes et al., 2009; Shah et al., 2021; Si & Ariya, 2018). Nevertheless, although much progress has been achieved in recent years, major aspects of atmospheric mercury chemistry are still not fully understood (Saiz-Lopez et al., 2020).

Atmospheric Hg^0 lifetime is around several months and therefore enters the stratosphere through tropical convective uplift (Horowitz et al., 2017). Mercury in the stratosphere is estimated to be about 20% of the total atmospheric Hg mass (Shah et al., 2021). Both elemental and oxidized mercury species have been measured directly in the stratosphere (Lyman et al., 2020; Lyman & Jaffe, 2012; Slemr et al., 2018; Talbot et al., 2007) or in air masses influenced by the stratosphere (e.g., Ebinghaus et al., 2007; Lyman & Jaffe, 2012; Radke et al., 2007). Early observations suggested that stratospheric mercury oxidation may be a significant sink for Hg^0 since a

Juan Carlos Gómez Martín, Joseph S. Francisco, John M. C. Plane
Software: Wuhu Feng, Daniel Roca-Sanjuán, Javier Carmona-García, Carlos A. Cuevas, Douglas E. Kinnison, Juan Carlos Gómez Martín, John M. C. Plane
Supervision: Alfonso Saiz-Lopez
Visualization: Anoop S. Mahajan
Writing – original draft: Alfonso Saiz-Lopez, A. Ulises Acuña, Anoop S. Mahajan, John M. C. Plane
Writing – review & editing: Alfonso Saiz-Lopez, A. Ulises Acuña, Anoop S. Mahajan, Juan Z. Dávalos, Daniel Roca-Sanjuán, Javier Carmona-García, Carlos A. Cuevas, Juan Carlos Gómez Martín, Joseph S. Francisco, John M. C. Plane

large fraction of the resulting gaseous oxidized mercury is expected to be taken up on aerosols irreversibly and removed from the stratosphere by sedimentation to the troposphere (Lyman & Jaffe, 2012). Indeed, stratospheric mercury-containing aerosols have also been observed, indicating that a fraction of mercury is partitioned into the particulate phase in the lower stratosphere (Murphy et al., 1998, 2006, 2014). However, more recent work reporting the most comprehensive set of measurements made over several years in the upper troposphere and lower stratosphere shows the presence of significant concentrations of stratospheric Hg^0 (0.25–0.7 ng/m^3) (Lyman et al., 2020; Slemr et al., 2018), which in turn implies the existence of efficient Hg reduction reactions, probably $Hg^{I,II}$ photoreduction (Saiz-Lopez et al., 2018, 2019). Despite this observational evidence for an active mercury redox chemical cycle in the stratosphere, most aspects of mercury chemistry in this region of the atmosphere remain unknown. This lack of fundamental knowledge prevents assessing the contribution of stratospheric mercury cycling and transport to the global biogeochemical cycle of the metal.

Here, we present a comprehensive photochemical mechanism for mercury oxidation in the stratosphere initiated by solar UV (253.7 nm) excitation of gas-phase atomic Hg, from its unreactive $^1S_0$ ground-state to the highly reactive triplet state, $Hg(^3P_1)$. The dominant deactivation channel of the excited triplet $Hg(^3P_1)$ should be collision with molecular oxygen to yield either mercuric oxide (HgO) or, by energy transfer to molecular oxygen, returning to the ground-state. The unstable HgO initiates a series of secondary reactions with chlorine species that ultimately yield stable water-soluble mercury halides such as $HgCl_2$. This new photochemical mechanism is further combined with the latest Hg chemical schemes to build the first stratospheric mercury chemistry model that describes the changes in the mercury oxidation chemistry as a function of altitude. We find that the new photosensitized chemistry dominates Hg oxidation above 35 km, with much faster rates than thermal, ground-state oxidation in the lower stratosphere. In addition, our results indicate that the overall Hg^0 oxidation to Hg^{II} in the stratosphere is controlled by chlorine and hydroxyl (OH) radical chemistry, being orders of magnitude faster than previously assumed mercury oxidation by bromine (Holmes et al., 2010; Horowitz et al., 2017; Lyman & Jaffe, 2012; Seigneur & Lohman, 2008; Slemr et al., 2018; Talbot et al., 2007).

2. Materials and Methods

2.1. Reaction Rate Coefficient Calculations

The rate coefficients and thermochemical values computed in this work, by a combination of electronic structure theory and Rice-Ramsperger-Kassel-Markus (RRKM) theory, are included in Table 1. For electronic structure calculations we used the hybrid density functional/Hartree−Fock B3LYP method from within the Gaussian 16 suite of programs (Frisch et al., 2016), together with Dunning's quadruple-ζ aug-cc-pVQZ correlation consistent basis, augmented with diffuse functions (Woon & Dunning, 1993). For Hg, the aug-cc-pVQZ basis set of Peterson and Puzzarini, (2005) was used. Molecular geometries were first optimized and checked for wave function stability, and their respective vibrational frequencies were calculated. The resulting geometries, rotational constants, vibrational frequencies, and energies of the stationary points on the potential energy surfaces of these reactions are listed in Table S1 in Supporting Information S1. Figure S1 in Supporting Information S1 illustrates the corresponding molecular geometries.

For the RRKM calculations, the Master Equation Solver for Multi-Energy well Reactions (MESMER) program (Glowacki et al., 2012) was used. Where applicable, a reaction is assumed to proceed via the formation of an excited adduct, which can either dissociate back to the reactants, be stabilized by collision with the third body into any minima on the potential energy surface, or dissociate to products. The internal energy of the adduct is divided into a contiguous set of grains (width 50 cm^{-1}), each containing a bundle of rovibrational states. Each grain is then assigned a set of microcanonical rate coefficients for dissociation back to the reactants or to the products, using inverse Laplace transformation to link them directly to the high-pressure limiting recombination coefficients. In the case of $Hg(^3P_1) + O_2$, this was set to $k_\infty = 3.0 \times 10^{-10}\ (T/298)^{0.167}$ cm^3 molecule^{-1} s^{-1} (Callear, 1987); for HgO + HCl, $k_\infty = 2.7 \times 10^{-10}\ (T/298)^{-0.17}$ cm^3 molecule^{-1} s^{-1}, the estimated dipole-dipole capture rate coefficient; and for OHgCl + HCl, $k_\infty = 2.0 \times 10^{-10}\ (T/298)^{0.17}$ cm^3 molecule^{-1} s^{-1}, a typical capture rate controlled by dispersion forces. The probability of collisional transfer between grains was estimated using the exponential down model: the average energy for downward transitions $\langle \Delta E \rangle_{down}$ was set to 300 cm^{-1}, typical of M = N_2 at 300 K, with a $T^{0.25}$ temperature dependence (Gilbert & Smith, 1990). The resulting temperature-dependent rate coefficients are listed in Table 1, together with the reaction energetics.

Table 1
New Gas-Phase Chemistry of Hg in the Stratosphere

Reaction	ΔH_r(0 K)/kJ mol^{-1}	k/cm^3 molecule^{-1} s^{-1}	Source
$Hg(^1S_0) + hv\ (\lambda = 253.7\ nm) \rightarrow Hg(^3P_1)$			(Kramida et al., 2018)
$Hg(^3P_1) \rightarrow Hg(^1S_0) + hv\ (\lambda = 253.7\ nm)$		$8.4 \times 10^6\ s^{-1}$	(Kramida et al., 2018)
$Hg(^3P_1) + N_2 \rightarrow Hg(^3P_0) + N_2$	−21.2	$5.1 \times 10^{-11} \exp(-701/T)$	(Callear & Shiundu, 1987)
$Hg(^3P_0) + O_2 \rightarrow Hg(^1S_0) + O_2(^3\Sigma_u^+)$	−27.0	$1.8 \times 10^{-10}\ (T/300)^{0.167}$	(Callear, 1987)
$Hg(^3P_1) + O_2 \rightarrow HgO(^3\Pi) + O$	−6.1	$1.7 \times 10^{-10}\ (T/300)^{0.53}$	[a] MESMER calculation on the PES in Figure S3 in Supporting Information S1
$Hg(^3P_1) + O_2 \rightarrow Hg(^1S_0) + O_2(^3\Sigma_u^+)$	−48.2	$1.3 \times 10^{-10}\ (T/300)^{-0.29}$	MESMER based on (Callear & Shiundu, 1987)
$HgO + O_2 \rightarrow Hg + O_3$	−72.4	$3.4 \times 10^{-13} \exp(-1993/T)$	[b] TST
$HgO + M \rightarrow Hg + O + M$	27.6	$8.4 \times 10^{-11} \exp(-3150/T)$	MESMER
$HgO + HCl \rightarrow HgCl + OH$	−64.6	$7.1 \times 10^{-11}(T/300)^{-1.14}$	MESMER calculation on the PES in Figure S4a in Supporting Information S1
$HgCl + O_3 \rightarrow OHgCl + O_2$	−184.0	$1.0 \times 10^{-10}\ (T/300)^{0.5}$	MESMER
$OHgCl + hv \rightarrow HgO + Cl\ (67\%) \rightarrow Hg + Cl + O\ (33\%)$			[c] Absorption cross sections and AINAMD simulations
$OHgCl + HCl \rightarrow HgCl_2 + OH$	−79.4	$7.9 \times 10^{-11}\ (T/300)^{-0.916}$	MESMER calculation on the PES in Figure S5 in Supporting Information S1
$OHgCl + CH_4 \rightarrow HOHgCl + CH_3$	−34	$1.5 \times 10^{-11} \exp(-1290/T)$	MESMER
$HOHgCl + hv \rightarrow Hg + OH + Cl\ (91\%)$			[c] Absorption cross sections and AINAMD simulations
$\rightarrow HgOH + Cl\ (6\%)$			
$\rightarrow HgCl + OH\ (3\%)$			
$HOHgCl + HCl \rightarrow HgCl_2 + H_2O$	−100	$1.3 \times 10^{-12}\ (T/300)^{-1.60}$	MESMER

[a]Master Equation Solver for Multi-Energy well Reactions (MESMER) program based on Rice-Ramsperger-Kassel-Markus (RRKM) theory. Potential Energy Surface (PES) is calculated based on Electronic Structure theory (Methods and Supporting Information S1). [b]Transition State Theory. [c]See Supporting Information S1 for computation details of absorption cross sections. The photolysis products and yields are determined by ab-initio non-adiabatic molecular dynamics (AINAMD) (Supporting Information S1).

Note that at the B3LYP level of theory, D_0(HgO) is 37 kJ mol^{-1}, which is consistent with earlier work (Filatov & Cremer, 2004). It is once electron correlation and spin-orbit coupling is included that the smaller bond energy has been determined (Filatov & Cremer, 2004; Peterson et al., 2007; Shepler & Peterson, 2003) (see Supporting Information S1).

2.2. Computation of Cross Sections and Photolysis Products of HOHgCl and OHgCl

A computational strategy documented and calibrated in previous works to determine ultraviolet and visible (UV-Vis) absorption spectra and cross sections of mercury compounds was reutilized here and adapted to HOHgCl, OHgCl, and $Hg(OH)_2$ (Francés-Monerris et al., 2020; Saiz-Lopez et al., 2018, 2019; Sitkiewicz et al., 2019). In addition, their photolysis yields upon light absorption in the stratosphere were determined by means of state-of-the-art *ab-initio* non-adiabatic molecular dynamic (AINAMD) simulations, previously applied to other atmospheric compounds (Carmona-García et al., 2021; Francés-Monerris et al., 2020). More details are provided in the Supporting Information S1.

2.3. Photochemical and Kinetics Model

We have developed a state-of-the-art photochemical and kinetics box model to study the effect of the different chemical pathways on Hg oxidation in the stratosphere. The model is based on the latest understanding of atmospheric Hg chemistry (Francés-Monerris et al., 2020; Saiz-Lopez et al., 2018; Shah et al., 2021) and also includes the new chemical and photochemical scheme proposed in this study (Table 1). The model is constrained with values of pressure, temperature, O_3, Br, Cl, OH, CH_4, CO, and HCl concentration profiles (Figure S2 in Supporting Information S1) from the Whole Atmosphere Community Climate Model (WACCM) (Neale et al., 2013). The stratospheric Hg^0

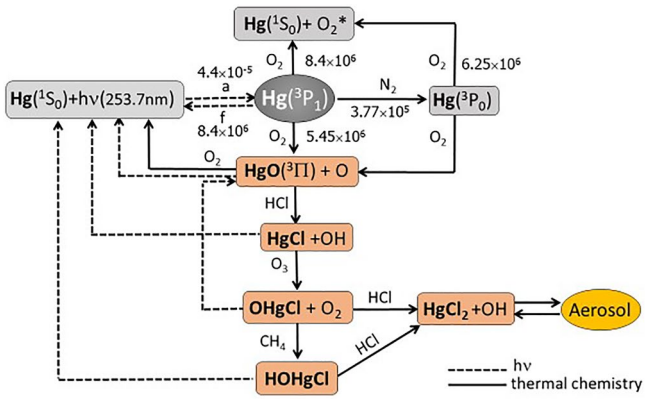

Figure 1. Photosensitized gas-phase oxidation of mercury in the stratosphere above the ozone layer for altitudes higher than ~35 km. The pseudo first-order rate coefficients for the primary reactions of the electronically excited $Hg(^3P_1)$ triplet state for these ambient conditions are shown in s^{-1}. The major, second-step chlorine-dependent oxidation reactions are also included.

concentration value is fixed at 0.5 ng m^{-3} (Slemr et al., 2018), assuming a well-mixed distribution through the column. The simultaneous differential equations describing the rate of change of each species (with rate coefficients in Table S2 in Supporting Information S1) are solved using the KPP 2.2.3 based Rosenbrock integrator (Damian et al., 2002). Photodissociation rates are calculated online using the latest cross sections with the TUV photolysis code (Madronich & Flocke, 1999). The model was run at every 5 km from the tropopause up to 60 km until steady state was reached. The model was run at 50°N 0°E for the month of June.

3. Results and Discussion

3.1. A Mechanism for Photosensitized Mercury Oxidation

In the chemical mechanism proposed here, atomic mercury is electronically excited from the relatively inert ground state Hg ($^1S_0$) to the highly reactive triplet state Hg ($^3P_1$) by solar radiation at 253.7 nm. In the Earth's atmosphere, these radiation conditions prevail above the stratospheric ozone layer maximum concentration (>35 km, 0.1–10 hPa, 220–260K) where the O_3 Hartley band is optically thin (see Supplementary Note 1 in Supporting Information S1) and the following photochemistry can take place (Figure 1):

$$Hg(^1S_0) + h\nu\,(\lambda = 253.7\text{nm}) \rightarrow Hg(^3P_1) \quad (1)$$

$$Hg(^3P_1) \rightarrow Hg(^1S_0) + h\nu(\lambda = 253.7\text{nm}) \quad (2)$$

$$Hg(^3P_1) + O_2 \rightarrow HgO(^3\Pi) + O \quad (3a)$$

$$\rightarrow Hg(^1S_0) + O_2{}^* \quad (3b)$$

$$Hg(^3P_1) + N_2 \rightarrow Hg(^3P_0) + N_2 \quad (4)$$

$$Hg(^3P_0) + O_2 \rightarrow Hg(^1S_0) + O_2{}^* \quad (5)$$

Primary reactions of electronically excited mercury atoms. The oscillator strength (f = 0.0243) for the $Hg(^1S_0) \rightarrow Hg(^3P_1)$ transition (R1) is relatively large (Kramida et al., 2018). Natural mercury contains seven stable isotopes, with masses 196–204 u and small differences in chemical reactivity (Bergquist & Blum, 2007; Sonke, 2011). Here, the rate of mercury excitation was computed based on a single absorption line with a Doppler linewidth of 0.03 cm^{-1} (0.93 GHz) at a temperature of 240 K, characteristic of the lower stratosphere, and a peak cross section of $\sigma = 7 \times 10^{-13}$ cm^2, derived from the f-value. Spontaneous emission from the Hg ($^3P_1$) triplet to the ground state (R2) is spin-forbidden and relatively slow (radiative lifetime of 119 ns, Einstein coefficient $A_{nm} = k_2 = 8.4 \times 10^6$ s^{-1}). Thus, for the specified stratospheric conditions the rate of radiative deactivation would be ca. 50% slower than the hard collision frequency (see below). The two additional Hg ($^3P_0$) and Hg ($^3P_2$) triplet components are dark metastable states with much longer lifetimes (Garstang, 1962).

The reaction of excited atomic mercury Hg ($^3P_1$) with O_2 (R3) has been studied for nearly a century, beginning with Gaviola's pioneering experiments on Hg-sensitized photochemistry (Gaviola, 1929), and reviewed several times (Burton & Noyes, 1969; Callear, 1987; Callear et al., 1959; Noyes & Leighton, 1941; Volman, 1963). The laboratory experiments show that the final reaction products are O_3 in large quantities (up to 60 molecules for each consumed mercury atom) (Volman, 1963) and HgO deposited as a solid film. However, the experiments did not establish unambiguously the path to HgO, and in particular the rate coefficient of the HgO primary reaction (R3a) could not be determined (See Supplementary Information, Part 1 in Supporting Information S1). In the present work the reaction rate coefficients were obtained from a combination of electronic structure and Rice-Ramsperger-Kassel-Marcus (RRKM) calculations, as detailed in Materials and Methods and Table 1. The R3a rate coefficient yielded a value of $k_{3a} = 1.7 \times 10^{-10}$ $(T/300)^{0.53}$ cm^3 $molecule^{-1}$ s^{-1}. Molecular geometries, rotational constants, vibrational frequencies, and energies computed by the quantum-chemical methods are listed in Table S1 in Supporting

Information S1. The Hg-O bond-energy obtained in this way (27.3 kJ mol^{-1}) is similar to previous predicted values, and in the spin-conserving reaction the mercury oxide would be produced as HgO($^3\Pi$) with little vibrational energy, ~6 kJ mol^{-1} (Supplementry Information and Figure S3 in Supporting Information S1), which is important for such a weakly bound molecule to survive in the stratospheric low-temperature environment.

The R3b step is just the transfer of electronic energy from atomic mercury to molecular oxygen (Figure S3 in Supporting Information S1) with a rate comparable to the collision frequency ($k_{coll} \sim 10^{-10}$ cm^3 molecule^{-1} s^{-1}, 240K) (Callear, 1987; Callear et al., 1959; Horiguchi & Tsuchiya, 1974; Volman, 1963). Triplet-triplet energy transfer experiments (Hippler et al., 1978) as well as O_3 synthesis cannot be explained unless the resultant excited oxygen molecule (O_2^*) is produced in a high-lying electronic state (***A,C*** or ***c*** (Michels, 1981)). In the present kinetic model, a value of $k_{3b} = 1.3 \times 10^{-10}$ (T/300)$^{-0.29}$ cm^3 molecule^{-1} s^{-1} is calculated based on previous experimental values (Callear & Shiundu, 1987).

Reaction 4, in which Hg($^3P_1$) is physically quenched by N_2, is well characterized with a rate constant $k_4 = 5.1 \times 10^{-11}$ exp (−701/T) cm^3 molecule^{-1} s^{-1} (Callear, 1987; Callear & Shiundu, 1987), and yields only the lowest metastable spin-orbit multiplet Hg($^3P_0$), which is 21.3 kJ mol^{-1} below Hg($^3P_1$). As discussed above, Hg($^3P_1$) can be quenched by O_2, with two possible channels yielding HgO or Hg($^1S_0$), respectively. Therefore, Hg($^3P_1$) is ~22 times more likely to be quenched by O_2 than N_2. Any Hg($^3P_0$) produced by R4 can be excited back to Hg($^3P_1$) by collisions with N_2, although this is very slow at atmospheric temperatures ($k(T) = 1.49 \times 10^{-10}$ exp (−3243/T) cm^3 molecule^{-1} s^{-1} (Callear & Shiundu, 1987). Much more likely is quenching of Hg($^3P_0 \rightarrow {}^1S_0$) by O_2 (R5), with a rate coefficient $k_5 = 1.8 \times 10^{-10}$ (T/300) $^{0.167}$ cm^3 molecule^{-1} s^{-1} (Callear, 1987) or chemical reaction to yield HgO, by analogy with R3a. The physical and chemical initial processes of elemental gas-phase mercury in the excited Hg($^3P_1$) triplet discussed above are shown in Figure 1, together with the estimated rates for the specified stratospheric conditions.

Second step reactions. HgO may be reduced back to elemental mercury by reaction with O_2 and by thermal- and photo-dissociation:

$$HgO(^3\Pi) + O_2 \rightarrow Hg + O_3 \quad (6)$$

$$HgO(^3\Pi) + M \rightarrow Hg + O + M \quad \text{(where M is primarily } N_2) \quad (7)$$

$$HgO(^3\Pi) + h\nu \rightarrow Hg + O \quad (8)$$

Reaction 6 is exothermic by 73 kJ mol^{-1} based on a bond energy for HgO($^3\Pi$) of 27 kJ mol^{-1}, but with a barrier of 15.4 kJ mol^{-1}, according to our calculations (see Figure S1 in Supporting Information S1 for a diagram of the transition state geometry and Figure S4b in Supporting Information S1 for the potential energy surface). A value of $k_6 = 3.4 \times 10^{-13}$ exp (−1993/T) cm^3 molecule^{-1} s^{-1} was computed as indicated above (Table 1). The thermal decomposition of the oxide (R7) in the gas phase is calculated to yield $k_7 = 8.4 \times 10^{-11}$ exp (−3150/T) cm^3 molecule^{-1} s^{-1}. The photo dissociation rate of the oxide back to atomic mercury has been computed based on the absorption spectrum and cross sections calculated before by high-level quantum mechanical methods (Saiz-Lopez et al., 2018).

We have also identified the following pathway for HgO($^3\Pi$) to form $HgCl_2$, the most stable form of oxidized Hg in the stratosphere:

$$HgO(^3\Pi) + HCl \rightarrow HgCl + OH \quad (9)$$

$$HgCl + O_3 \rightarrow OHgCl + O_2 \quad (10)$$

$$OHgCl + HCl \rightarrow HgCl_2 + OH \quad (11)$$

$$\begin{aligned} OHgCl + h\nu &\rightarrow HgO + Cl \quad (67\%) \\ &\rightarrow Hg + Cl + O \quad (33\%) \end{aligned} \quad (12)$$

When HgO($^3\Pi$) reacts with HCl, a weakly bound HgO-HCl complex forms initially on the spin-conserving triplet surface (Figure S4a in Supporting Information S1), which rearranges over a slight barrier (1 kJ mol^{-1}) to the more stable HgCl-OH complex. This can then dissociate either to HgCl + OH (99%) or HgOH + Cl (1%), in accord

with the relative energies (Figure S4a in Supporting Information S1). The rate coefficient computed here is close to the collisional limit, $k_9 = 7.1 \times 10^{-11} (T/300)^{-1.14}$ cm^3 molecule^{-1} s^{-1}. For the reaction of HgCl with O_3 there is no obvious barrier, and the formation of OHgCl is quite exothermic ($\Delta H_0 = -184$ kJ mol^{-1}). We therefore assign this reaction a rate coefficient set to a collision frequency with a $T^{0.5}$ dependence to yield $k_{10} = 1 \times 10^{-10} (T/300)^{0.5}$ cm^3 molecule^{-1} s^{-1} (Table 1). Reaction 11 is also exothermic, with $\Delta H_0 = -79.4$ kJ mol^{-1}, and the potential energy surface (Figure S5 in Supporting Information S1) is similar to that of HgO + HCl (Figure S4a in Supporting Information S1). In this case, 99% of the reaction product is $HgCl_2$ rather than HOHgCl, again following the more exothermic pathway. A rate coefficient of $k_{11} = 7.9 \times 10^{-11} (T/300)^{-0.916}$ cm^3 molecule^{-1} s^{-1} is calculated. Photolytic dissociation of the OHgCl radical (R12) yields mainly (67%) HgO + Cl (Table S3 in Supporting Information S1), which will then recycle to $HgCl_2$ by reactions R9–R11, as predicted by the absorption cross section (Figure S6 in Supporting Information S1) and photodissociation dynamics computed here.

An additional pathway for the formation of $HgCl_2$ results from the abstraction reaction shown below:

$$OHgCl + CH_4 \rightarrow HOHgCl + CH_3 \quad (13)$$

$$HOHgCl + HCl \rightarrow HgCl_2 + H_2O \quad (14)$$

$$\begin{aligned} HOHgCl + h\nu &\rightarrow Hg + OH + Cl \ (91\%) \\ &\rightarrow HgOH + Cl \ (6\%) \\ &\rightarrow HgCl + OH \ (3\%) \end{aligned} \quad (15)$$

The calculated rate coefficient for R13 of $k_{13} = 1.5 \times 10^{-11} \exp(-1290/T)$ cm^3 molecule^{-1} s^{-1} indicates that this abstraction reaction should be quite slow at stratospheric temperatures. Thus, at 220 K the rate of the competing R11 is 2,500 times faster. In any case, even if it does happen, the resulting HOHgCl product would react with HCl to yield $HgCl_2$ (R14) as this reaction is exothermic (−100 kJ mol^{-1}), with a calculated rate coefficient of $k_{14} = 1.3 \times 10^{-12} (T/300)^{-1.6}$ cm^3 molecule^{-1} s^{-1}. The corresponding absorption cross section (Figure S7 in Supporting Information S1) and photodissociation products (Table S4 in Supporting Information S1) of HOHgCl photolysis (R15) were also calculated to evaluate its contribution to the present mechanism. Finally, the possible direct reaction of mercury oxide with H_2O vapor was found to be unimportant for these specific reaction conditions (see Supplementary Note 2 in Supporting Information S1). Similarly, we studied the effect of the reaction between $Hg(^3P_1)$ and H_2O (Pertel & Gunning, 1959) to make HgOH followed by reaction with HCl to HgCl (Guzman & Bozzelli, 2019) and found their contribution to be negligible to total oxidized mercury (Supplementary Note 2 in Supporting Information S1).

3.2. Quantitative Model of the Chemical Cycle of Mercury in the Stratosphere

There is currently no established model of the gas-phase chemical reactions of Hg^0, $Hg^{I,}$ and Hg^{II} species in the stratosphere, therefore, we build for the first time a quantitative photochemistry and kinetics model of stratospheric mercury (Section 2, and Supporting Information S1). The model includes the state-of-the-art chemical schemes developed to explain mercury chemistry in the troposphere based on bromine-, chlorine, and OH-initiated Hg oxidation (Francés-Monerris et al., 2020; Saiz-Lopez et al., 2020; Shah et al., 2021) along with the new chemistry presented here (Table S2 in Supporting Information S1). There is a sharp transition in the metal oxidation mechanism from altitudes above the ozone layer, where the Hg-photosensitized reactions are dominant, to those below the ozone layer, where thermal reactions take the control. These large differences are accounted for in the model, which is consistent also with established tropospheric Hg chemistry and simulations, and agrees with previous works (e.g., Shah et al., 2021). Hence, the new model represents a unified model of mercury chemistry that bridges chemistry both in the troposphere and stratosphere.

Figure 2 shows the simulation results at 50°N in June as a function of altitude, where the tropopause ranges between 12 and 14 km and the stratopause is approximately at 50 km. Below 35 km, where photosensitized oxidation does not occur, reaction with the radical OH drives the initial loss rate of gas-phase elemental mercury (Figure 2a). In that same region (15–35 km), the overall conversion of elemental to oxidized mercury is dominated by both OH and chlorine oxidation (Figure 2c). This is because, in addition to the faster initial OH oxidation, the contribution of the OH channel is enhanced (Figure 2b) by the slow photodissociation rate of the final

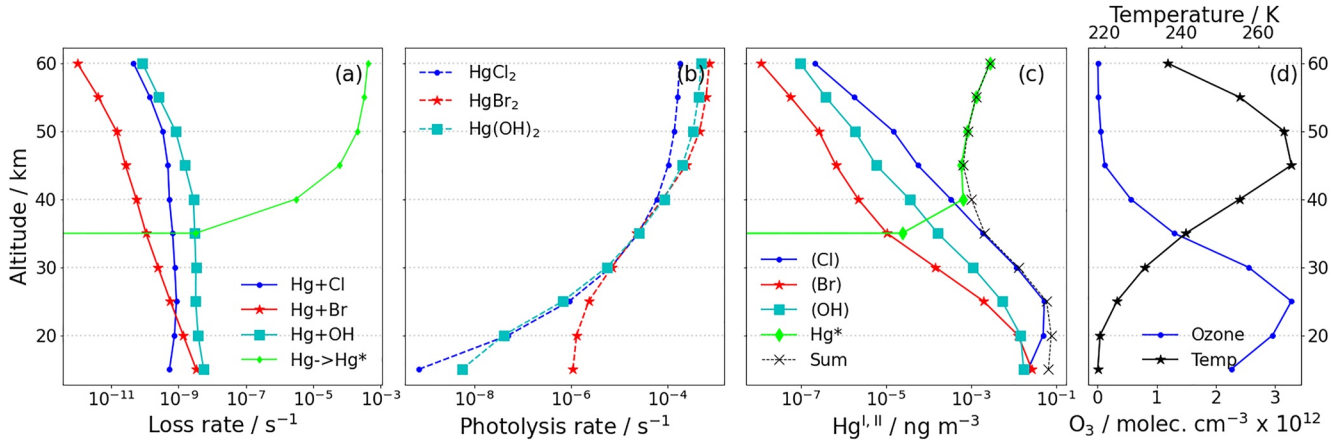

Figure 2. Model predictions for the different gas-phase oxidation mechanisms of elemental Hg^0 in the stratosphere developed here as a function of altitude, for 50°N, 0°E, June. (a) Initial Hg^0 loss rate due to reaction with Cl, Br, and OH, represented by the corresponding pseudo first-order rate coefficient (s^{-1}), as a function of the concentration of these species. The initial loss rate of the excited $Hg(^3P_1)$ triplet is also shown. (b) Photolysis rates (s^{-1}) of the main Hg^{II} compounds that result from mercury oxidation. (c) Vertical concentration profile of the $Hg^{I,II}$ species containing X = Cl, Br, OH. (d) Temperature and ozone number density.

oxidized product $Hg(OH)_2$, as computed here from its UV absorption cross section (Figure S8 in Supporting Information S1). Similarly, $HgCl_2$ has a long lifetime against photolysis (Figure 2b). This results in $HgCl_2$ and $Hg(OH)_2$ being the dominant reservoirs for oxidized Hg in the lower stratosphere (Figure 2b; Figure S9 in Supporting Information S1). In sharp contrast, Figure 2 also shows that in the upper stratosphere, above approximately 35 km, Hg^0 loss is entirely driven by the photosensitized oxidation of Hg^0 to HgO, followed by reactions with HCl to form $HgCl_2$, which is the main oxidized mercury species in the mid to upper stratosphere (Figure S9 in Supporting Information S1). Note that the initial rate of Hg oxidation by this new photosensitized chemistry in the mid-to upper stratosphere is 10^3–10^4 times faster than the combined rates of Hg oxidation by bromine, chlorine, and OH radical (Figure 2a). The halide $HgCl_2$, which is the main final oxidation product from the reaction of electronically excited Hg, is photolyzed rapidly back to Hg^0 in the mid-to upper-stratosphere. Hence, Hg^0 and $HgCl_2$ exist in a pseudo steady-state, which is tilted toward $HgCl_2$ due to the oxidation rate being about 2 times faster than the photolysis of $HgCl_2$. The modeled partitioning of oxidized mercury species as a function of altitude is shown in Figure S9 in Supporting Information S1. Observations of mercury species have been made in the stratosphere onboard the IAGOS-CARIBIC aircraft and show the prevalence of about 0.5 ng m^{-3} Hg^0 up to 4 km above the thermal tropopause (Slemr et al., 2018). If the model is initialized with this value, it predicts ~0.1 ng m^{-3} of $Hg^{I,II}$, which matches well with the observed difference between total mercury and Hg^0 (0.17 ng m^{-3}) in this region (Slemr et al., 2018).

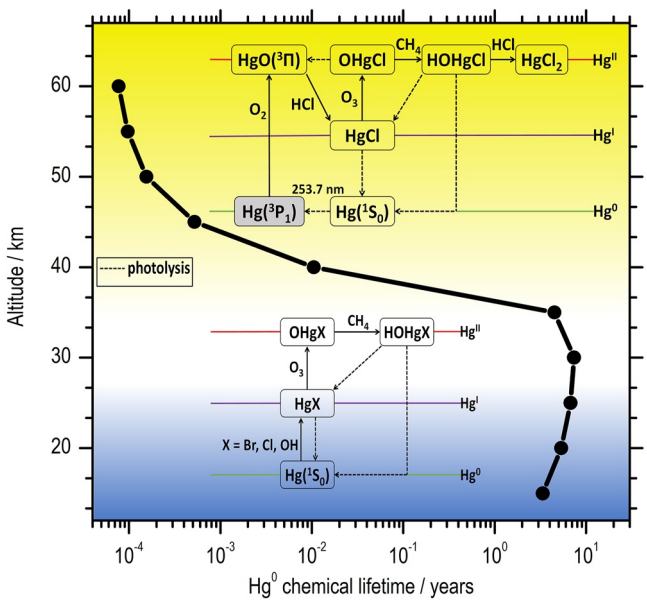

Figure 3. The lifetime of elemental mercury against chemical loss as a function of altitude in the stratosphere for 50°N, 0°E, June. In the middle to upper stratosphere Hg oxidation is dominated by fast reactions of the UV-excited $Hg(^3P_1)$ triplet state, which transform elemental mercury directly into Hg^{II} compounds (see inset), resulting in short chemical lifetimes of elemental mercury in the day-hour range. However, in the lower stratosphere, Hg triplet excitation at 254 nm by solar radiation is blocked by the ozone Hartley band with maximum absorption at the same wavelength. Therefore, ground-state unreactive atomic Hg^0 is slowly oxidized by thermal reactions with Cl, Br, and OH species to yield Hg^I intermediate compounds (see inset). In addition, secondary photoreduction processes revert many of the oxidized products back to elemental mercury, resulting finally in Hg^0 chemical lifetimes in the years range in the lower stratosphere.

4. Conclusions

The different Hg oxidation mechanisms reveal two very distinct mercury chemistry regimes in the stratosphere, one above the ozone layer where $Hg(^3P_1)$ photosensitization drives fast oxidation, and the other below the ozone layer controlled by ground-state initiated slow oxidation. As noted above, this is a consequence of the fortuitous coincidence of the absorption maxima at 254 nm of both, the mercury excitation transition $Hg(^1S_0) \rightarrow Hg(^3P_1)$ and the ozone Hartley absorption band. As shown in Figure 3, the large difference in the rates of Hg oxidation in these two stratospheric chemical regimes leads to a significant impact on the lifetime of Hg^0 against chemical loss

throughout the stratosphere. Thus, the Hg^0 chemical lifetime ranges from years in the lower stratosphere to days and even hours in the mid-to upper-stratosphere (Figure 3). The long lifetime of Hg^0 calculated here for the lower stratosphere, and also inferred from observations (Slemr et al., 2018), would enable the steady flow of mercury to the upper stratosphere where photosensitized oxidation is extremely efficient. The calculated Hg^0 lifetime of hours in the upper stratosphere is only comparable to the atmospheric mercury depletion events measured in the Arctic springtime boundary layer (Schroeder et al., 1998). However, unlike the localized and episodic nature of these Arctic events, the mechanism proposed here indicates that the lifetime of elemental mercury against chemical loss would be of only hours throughout the global mid to upper stratosphere.

Our study shows that the chemical cycling of mercury in the stratosphere is much more active and complex than previously anticipated. The new chemical scheme presented here results in stratosphere mercury oxidation rates orders of magnitude faster than currently assumed, which change sharply as a function of altitude. Atmospheric Hg oxidation has so far been considered to be initiated only from the Hg ground electronic state, which also requires to proceed via intermediate Hg^I species (Shah et al., 2021). We show here that stratospheric Hg oxidation can also proceed by an alternative Hg photosensitized chemistry, allowing efficient oxidation of Hg^0 directly to Hg^{II}. The novel mercury chemical and photochemical framework reported herein has broad implications for the stratospheric mercury residence time and its global dispersion. This new fundamental chemistry provides for the first time a quantitative mechanism of mercury chemistry in the stratosphere and reveals this region of the atmosphere as a unique environment for Hg chemical cycling.

Data Availability Statement

The software code for the WACCM model is available from https://www.cesm.ucar.edu/models/. The software code for the TUV Photolysis code is available from https://www2.acom.ucar.edu/modeling/tropospheric-ultraviolet-and-visible-tuv-radiation-model. All study data are included in the article and/or SI Appendix. Data related to this article are also available in Mendeley https://doi.org/10.17632/36jv45t26k.1.

Acknowledgments
This study has received funding from the European Research Council Executive Agency under the European Union's Horizon 2020 Research and Innovation programme (Project 'ERC-2016-COG726349 CLIMAHAL'). The project that gave rise to these results received the support of a fellowship for J.C.-G. from "la Caixa" Foundation (ID 100010434); the fellowship code is LCF/BQ/DR20/11790027. D.R.-S. is thankful to the Spanish Ministerio de Ciencia e Innovación/Fondos Europeos de Desarrollo Regional (MICINN/FEDER) for financial support through the project CTQ2017-87054-C2-2-P and the Ramón y Cajal fellowship (RYC-2015-19234).

References

AMAP/U.N. (2019). Technical Background Report for the Global Mercury Assessment 2018. *Arctic Monitoring and Assessment Programme/UN Environment Programme, Chemicals and Health Branch*, Geneva, Switzerland. Viii + 426 Pp Including E-A.

Bergquist, B. A., & Blum, J. D. (2007). Mass-dependent and -independent fractionation of Hg isotopes by photoreduction in aquatic systems. *Science*, *318*(5849), 417–420. https://doi.org/10.1126/science.1148050

Burton, C., & Noyes, W. (1969). Chapter 1 effect of low energy radiation. *Comprehensive Chemical Kinetics*, *3*, 1–66.

Callear, A. B. (1987). Excited mercury complexes. *Chemical Reviews*, *87*(2), 335–355. https://doi.org/10.1021/cr00078a004

Callear, A. B., Patrick, C. R., & Robb, J. C. (1959). The reaction of excited mercury (Hg 63P1) with oxygen. *Transactions of the Faraday Society*, *55*(0), 280–287. https://doi.org/10.1039/TF9595500280

Callear, A. B., & Shiundu, P. M. (1987). Temperature dependence of the Hg 6s6p(3P0→3P1) transition induced by nitrogen. *Chemical Physics Letters*, *136*(3), 342–345. https://doi.org/10.1016/0009-2614(87)80263-4

Carmona-García, J., Francés-Monerris, A., Cuevas, C. A., Trabelsi, T., Saiz-Lopez, A., Francisco, J. S., & Roca-Sanjuán, D. (2021). Photochemistry and non-adiabatic photodynamics of the HOSO radical. *Journal of the American Chemical Society*, *143*(29), 10836–10841. https://doi.org/10.1021/jacs.1c05149

Damian, V., Sandu, A., Damian, M., Potra, F., & Carmichael, G. R. (2002). The kinetic preprocessor KPP-a software environment for solving chemical kinetics. *Computers & Chemical Engineering*, *26*(11), 1567–1579. https://doi.org/10.1016/S0098-1354(02)00128-X

Driscoll, C. T., Mason, R. P., Chan, H. M., Jacob, D. J., & Pirrone, N. (2013). Mercury as a global pollutant: Sources, pathways, and effects. *Environmental Science and Technology*, *47*(10), 4967–4983. https://doi.org/10.1021/es305071v

Ebinghaus, R., Slemr, F., Brenninkmeijer, C. A. M., van Velthoven, P., Zahn, A., Hermann, M., et al. (2007). Emissions of gaseous mercury from biomass burning in South America in 2005 observed during CARIBIC flights. *Geophysical Research Letters*, *34*(8). https://doi.org/10.1029/2006GL028866

Filatov, M., & Cremer, D. (2004). Revision of the dissociation energies of mercury chalcogenides—Unusual types of mercury bonding. *ChemPhysChem*, *5*(10), 1547–1557. https://doi.org/10.1002/cphc.200301207

Francés-Monerris, A., Carmona-García, J., Acuña, A. U., Dávalos, J. Z., Cuevas, C. A., Kinnison, D. E., et al. (2020). Photodissociation mechanisms of major mercury(II) species in the atmospheric chemical cycle of mercury. *Angewandte Chemie International Edition*, *59*(19), 7605–7610. https://doi.org/10.1002/anie.201915656

Frisch, M. J., Trucks, G. W., Schlegel, H. B., Scuseria, G. E., Robb, M. A., Cheeseman, J. R., et al. (2016). *Gaussian 16*. Rev. C.01.

Garstang, R. H. (1962). Hyperfine structure and intercombination line intensities in the spectra of magnesium, zinc, cadmium, and Mercury$\ast$. *Journal of the Optical Society of America*, *52*(8), 845–851. https://doi.org/10.1364/JOSA.52.000845

Gaviola, E. (1929). The efficiency of quenching collisions and the radius of the excited mercury atom. *Physics Review*, *33*(3), 309–318. https://doi.org/10.1103/PhysRev.33.309

Gilbert, R. G., & Smith, S. C. (1990). *Theory of unimolecular and recombination reactions*. Blackwell.

Glowacki, D. R., Liang, C.-H., Morley, C., Pilling, M. J., & Robertson, S. H. (2012). MESMER: An open-source master equation solver for multi-energy well reactions. *The Journal of Physical Chemistry A*, *116*(38), 9545–9560. https://doi.org/10.1021/jp3051033

Gustin, M. S., Amos, H. M., Huang, J., Miller, M. B., & Heidecorn, K. (2015). Measuring and modeling mercury in the atmosphere: A critical review. *Atmospheric Chemistry and Physics*, *15*(10), 5697–5713. https://doi.org/10.5194/acp-15-5697-2015

Guzman, F. J., & Bozzelli, J. (2019). Thermodynamics of OHgX, XHgOH, XHgOCl, XHgOBr, and HOHgY gaseous oxidized mercury molecules from isodesmic, isogyric, and atomization work reactions (X = halogen, Y = OH, OCl, OBr). *The Journal of Physical Chemistry A*, *123*(20), 4452–4464. https://doi.org/10.1021/acs.jpca.9b01358

Hippler, H., Wendt, H. R., & Hunziker, H. E. (1978). Excited intermediates in the Hg-photosensitized reaction of O2 detected by energy transfer. *The Journal of Chemical Physics*, *68*(11), 5103–5111. https://doi.org/10.1063/1.435610

Holmes, C. D., Jacob, D. J., Corbitt, E. S., Mao, J., Yang, X., Talbot, R., & Slemr, F. (2010). Global atmospheric model for mercury including oxidation by bromine atoms. *Atmospheric Chemistry and Physics*, *10*(24), 12037–12057. https://doi.org/10.5194/acp-10-12037-2010

Horiguchi, H., & Tsuchiya, S. (1974). Quenching of excited mercury atoms(63P1 and 63P0) in molecular collisions. *Bulletin of the Chemical Society of Japan*, *47*(11), 2768–2774. https://doi.org/10.1246/bcsj.47.2768

Horowitz, H. M., Jacob, D. J., Zhang, Y., Dibble, T. S., Slemr, F., Amos, H. M., et al. (2017). A new mechanism for atmospheric mercury redox chemistry: Implications for the global mercury budget. *Atmospheric Chemistry and Physics*, *17*(10), 6353–6371. https://doi.org/10.5194/acp-17-6353-2017

Hynes, A. J., Donohoue, D. L., Goodsite, M. E., & Hedgecock, I. M. (2009). Our current understanding of major chemical and physical processes affecting mercury dynamics in the atmosphere and at the air-water/terrestrial interfaces. In R. Mason, & N. Pirrone (Eds.), *Mercury fate and transport in the global atmosphere: Emissions, measurements and models* (pp. 427–457). Springer US. https://doi.org/10.1007/978-0-387-93958-2_14

Jiskra, M., Heimbürger-Boavida, L.-E., Desgranges, M.-M., Petrova, M. V., Dufour, A., Ferreira-Araujo, B., et al. (2021). Mercury stable isotopes constrain atmospheric sources to the ocean. *Nature*, *597*(7878), 678–682. https://doi.org/10.1038/s41586-021-03859-8

Kramida, A., Ralchenko, Y., Reader, J., & Team, N. A. (2018). *NIST Atomic Spectra Database* (Vol. 78). National Institute of Standards and Technology. https://doi.org/10.18434/T4W30F

Lyman, S. N., Cheng, I., Gratz, L. E., Weiss-Penzias, P., & Zhang, L. (2020). An updated review of atmospheric mercury. *The Science of the Total Environment*, *707*, 135575. https://doi.org/10.1016/j.scitotenv.2019.135575

Lyman, S. N., & Jaffe, D. A. (2012). Formation and fate of oxidized mercury in the upper troposphere and lower stratosphere. *Nature Geoscience*, *5*(2), 114–117. https://doi.org/10.1038/ngeo1353

Madronich, S., & Flocke, S. (1999). The role of solar radiation in atmospheric chemistry. In P. Boule (Ed.), *Environmental photochemistry. The handbook of, Environmental chemistry (reactions and processes)* (Vol. 2/2L). Springer. https://doi.org/10.1007/978-3-540-69044-3_1

Michels, H. H. (1981). Electronic structure of excited states of selected atmospheric systems. In *Advances in chemical physics* (pp. 225–340). John Wiley & Sons, Ltd. https://doi.org/10.1002/9780470142646.ch3

Murphy, D. M., Froyd, K. D., Schwarz, J. P., & Wilson, J. C. (2014). Observations of the chemical composition of stratospheric aerosol particles. *Quarterly Journal of the Royal Meteorological Society*, *140*(681), 1269–1278. https://doi.org/10.1002/qj.2213

Murphy, D. M., Hudson, P. K., Thomson, D. S., Sheridan, P. J., & Wilson, J. C. (2006). Observations of mercury-containing aerosols. *Environmental Science and Technology*, *40*(10), 3163–3167. https://doi.org/10.1021/es052385x

Murphy, D. M., Thomson, D. S., & Mahoney, M. J. (1998). In situ measurements of organics, meteoritic material, mercury, and other elements in aerosols at 5 to 19 kilometers. *Science*, *282*(5394), 1664–1669. https://doi.org/10.1126/science.282.5394.1664

Neale, R. B., Richter, J., Park, S., Lauritzen, P. H., Vavrus, S. J., Rasch, P. J., & Zhang, M. (2013). The mean climate of the community atmosphere model (CAM4) in forced SST and fully coupled experiments. *Journal of Climate*, *26*(14), 5150–5168. https://doi.org/10.1175/JCLI-D-12-00236.1

Noyes, W. A., & Leighton, P. A. (1941). Photochemistry of gases. *American Chemical Society*, *19*(14), 809. https://doi.org/10.1021/cen-v019n014.p809.News Edition

Obrist, D., Kirk, J. L., Zhang, L., Sunderland, E. M., Jiskra, M., & Selin, N. E. (2018). A review of global environmental mercury processes in response to human and natural perturbations: Changes of emissions, climate, and land use. *Ambio*, *47*(2), 116–140. https://doi.org/10.1007/s13280-017-1004-9

Pertel, R., & Gunning, H. E. (1959). Photochemiscal separation of mercury isotopes: II. The reaction of Hg_20_2(3P1) atoms, photoexcited in natural mercury vapor, with water vapor and other HgO-forming substrates. *Canadian Journal of Chemistry*, *37*(1), 35–42. https://doi.org/10.1139/v59-007

Peterson, K. A., & Puzzarini, C. (2005). Systematically convergent basis sets for transition metals. II. Pseudopotential-based correlation consistent basis sets for the group 11 (Cu, Ag, Au) and 12 (Zn, Cd, Hg) elements. *Theoretical Chemistry Accounts*, *114*(4), 283–296. https://doi.org/10.1007/s00214-005-0681-9

Peterson, K. A., Shepler, B. C., & Singleton, J. M. (2007). The group 12 metal chalcogenides: An accurate multireference configuration interaction and coupled cluster study. *Molecular Physics*, *105*(9), 1139–1155. https://doi.org/10.1080/00268970701241664

Radke, L. F., Friedli, H. R., & Heikes, B. G. (2007). Atmospheric mercury over the NE Pacific during spring 2002: Gradients, residence time, upper troposphere lower stratosphere loss, and long-range transport. *Journal of Geophysical Research*, *112*(D19). D19305. https://doi.org/10.1029/2005JD005828

Saiz-Lopez, A., Acuña, A. U., Trabelsi, T., Carmona-García, J., Dávalos, J. Z., Rivero, D., et al. (2019). Gas-phase photolysis of Hg(I) radical species: A new atmospheric mercury reduction process. *Journal of the American Chemical Society*, *141*(22), 8698–8702. https://doi.org/10.1021/jacs.9b02890

Saiz-Lopez, A., Sitkiewicz, S. P., Roca-Sanjuán, D., Oliva-Enrich, J. M., Dávalos, J. Z., Notario, R., et al. (2018). Photoreduction of gaseous oxidized mercury changes global atmospheric mercury speciation, transport and deposition. *Nature Communications*, *9*(1), 4796. https://doi.org/10.1038/s41467-018-07075-3

Saiz-Lopez, A., Travnikov, O., Sonke, J. E., Thackray, C. P., Jacob, D. J., Carmona-García, J., et al. (2020). Photochemistry of oxidized Hg(I) and Hg(II) species suggests missing mercury oxidation in the troposphere. *Proceedings of the National Academy of Sciences*, *117*(49), 30956–30949. LP – 30956. https://doi.org/10.1073/pnas.1922486117

Schroeder, W. H., Anlauf, K. G., Barrie, L. A., Lu, J. Y., Steffen, A., Schneeberger, D. R., & Berg, T. (1998). Arctic springtime depletion of mercury. *Nature*, *394*(6691), 331–332. https://doi.org/10.1038/28530

Seigneur, C., & Lohman, K. (2008). Effect of bromine chemistry on the atmospheric mercury cycle. *Journal of Geophysical Research*, *113*(D23). D23309. https://doi.org/10.1029/2008JD010262

Shah, V., Jacob, D. J., Thackray, C. P., Wang, X., Sunderland, E. M., Dibble, T. S., et al. (2021). Improved mechanistic model of the atmospheric redox chemistry of mercury. *Environmental Science \& Technology*, 14445–14456. null. https://doi.org/10.1021/acs.est.1c03160

Shepler, B. C., & Peterson, K. A. (2003). Mercury monoxide: A systematic investigation of its ground electronic state. *The Journal of Physical Chemistry A*, *107*(11), 1783–1787. https://doi.org/10.1021/jp027512f

Si, L., & Ariya, P. A. (2018). Recent advances in atmospheric chemistry of mercury. *Atmosphere*, *9*(2), 76. https://doi.org/10.3390/atmos9020076
Sitkiewicz, S. P., Rivero, D., Oliva-Enrich, J. M., Saiz-Lopez, A., & Roca-Sanjuán, D. (2019). Ab initio quantum-chemical computations of the absorption cross sections of HgX2 and HgXY (X, Y= Cl, Br, and I: Molecules of interest in the Earth's atmosphere. *Phys. Chem. Chem. Phys.*, *21*(1), 455–467. https://doi.org/10.1039/C8CP06160B
Slemr, F., Weigelt, A., Ebinghaus, R., Bieser, J., Brenninkmeijer, C. A. M., Rauthe-Schöch, A., et al. (2018). Mercury distribution in the upper troposphere and lowermost stratosphere according to measurements by the IAGOS-CARIBIC observatory: 2014--2016. *Atmospheric Chemistry and Physics*, *18*(16), 12329–12343. https://doi.org/10.5194/acp-18-12329-2018
Sonke, J. E. (2011). A global model of mass independent mercury stable isotope fractionation. \gca, *75*(16), 4577–4590. https://doi.org/10.1016/j.gca.2011.05.027
Talbot, R., Mao, H., Scheuer, E., Dibb, J., & Avery, M. (2007). Total depletion of Hg° in the upper troposphere–lower stratosphere. *Geophysical Research Letters*, *34*(23). https://doi.org/10.1029/2007GL031366
Volman, D. H. (1963). Photochemical gas phase reactions in the hydrogen-oxygen system. In *Advances in photochemistry* (pp. 43–82). John Wiley & Sons, Ltd. https://doi.org/10.1002/9780470133316.ch3
Woon, D. E., & Dunning, T. H. (1993). Gaussian basis sets for use in correlated molecular calculations. III. The atoms aluminum through argon. *The Journal of Chemical Physics*, *98*(2), 1358–1371. https://doi.org/10.1063/1.464303

References From the Supporting Information

Adamo, C., & Barone, V. (1999). Toward reliable density functional methods without adjustable parameters: The PBE0 model. *The Journal of Chemical Physics*, *110*(13), 6158–6170. https://doi.org/10.1063/1.478522
Andrae, D., Häußermann, U., Dolg, M., Stoll, H., & Preuß, H. (1990). Energy-adjustedab initio pseudopotentials for the second and third row transition elements. *Theoretica Chimica Acta*, *77*(2), 123–141. https://doi.org/10.1007/BF01114537
Aquilante, F., Autschbach, J., Baiardi, A., Battaglia, S., Borin, V. A., Chibotaru, L. F., et al. (2020). Modern quantum chemistry with [Open] Molcas. *The Journal of Chemical Physics*, *152*(21), 214117. https://doi.org/10.1063/5.0004835
Balabanov, N. B., Shepler, B. C., & Peterson, K. A. (2005). Accurate global potential energy surface and reaction dynamics for the ground state of HgBr2. *The Journal of Physical Chemistry A*, *109*(39), 8765–8773. https://doi.org/10.1021/jp053415l
Barbatti, M., Aquino, A. J. A., & Lischka, H. (2010). The UV absorption of nucleobases: Semi-classical ab initio spectra simulations. *Phys. Chem. Chem. Phys.*, *12*(19), 4959–4967. https://doi.org/10.1039/B924956G
Barbatti, M., Granucci, G., Ruckenbauer, M., & Pittner, J. (2007). Newton-X: A package for Newtonian dynamics close to the crossing seam. *Dynamics*, *16*, 3.
Barbatti, M., Ruckenbauer, M., Plasser, F., Pittner, J., Granucci, G., Persico, M., & Lischka, H. (2014). Newton-X: A surface-hopping program for nonadiabatic molecular dynamics. *WIREs Computational Molecular Science*, *4*(1), 26–33. https://doi.org/10.1002/wcms.1158
Barrera, J. A., Fernandez, R. P., Iglesias-Suarez, F., Cuevas, C. A., Lamarque, J.-F., & Saiz-Lopez, A. (2020). Seasonal impact of biogenic very short-lived bromocarbons on lowermost stratospheric ozone between 60oN and 60oS during the 21st century. *Atmospheric Chemistry and Physics*, *20*(13), 8083–8102. https://doi.org/10.5194/acp-20-8083-2020
Carmona-García, J., Trabelsi, T., Francés-Monerris, A., Cuevas, C. A., Saiz-Lopez, A., Roca-Sanjuán, D., & Francisco, J. S. (2021). Photochemistry of HOSO2 and SO3 and implications for the production of sulfuric acid. *Journal of the American Chemical Society*, *143*(44), 18794–18802. https://doi.org/10.1021/jacs.1c10153
Carpenter, L. J., MacDonald, S. M., Shaw, M. D., Kumar, R., Saunders, R. W., Parthipan, R., et al. (2013). Atmospheric iodine levels influenced by sea surface emissions of inorganic iodine. *Nature Geoscience*, *6*(2), 108–111. https://doi.org/10.1038/ngeo1687
ChaChCChaChaChChase, M. W. J., Davies, C. A., Downey, J. R. J., Frurip, D. J., McDonald, R. A., *& Syverud, A. N. (1985). NIST JANAF THERMOCHEMICAL TABLES 1985 version 1.0*. National Institute of Standards and Technology.
Crespo-Otero, R., & Barbatti, M. (2012). Spectrum simulation and decomposition with nuclear ensemble: Formal derivation and application to benzene, furan and 2-phenylfuran. *Theoretical Chemistry Accounts*, *131*(6), 1237. https://doi.org/10.1007/s00214-012-1237-4
de Macedo, L. G. M., Oliveira, C. A., Gomes, J. S., Alves, C. N., de Souza, A. R., Pimentel, A. S., & Gargano, R. (2011). *Journal of computational and theoretical nanoscience*. Retrieved from https://www.ingentaconnect.com/content/asp/jctn/2011/00000008/00000001/art00007. Fully relativistic 4-components DFT investigation on bonding and dissociation energy of HgO
Dibble, T. S., Tetu, H. L., Jiao, Y., Thackray, C. P., & Jacob, D. J. (2020). Modeling the OH-initiated oxidation of mercury in the global atmosphere without violating physical laws. *The Journal of Physical Chemistry A*, *124*(2), 444–453. https://doi.org/10.1021/acs.jpca.9b10121
Dibble, T. S., Zelie, M. J., & Mao, H. (2012). Thermodynamics of reactions of ClHg and BrHg radicals with atmospherically abundant free radicals. *Atmospheric Chemistry and Physics*, *12*(21), 10271–10279. https://doi.org/10.5194/acp-12-10271-2012
Donohoue, D. L., Bauer, D., Cossairt, B., & Hynes, A. J. (2006). Temperature and pressure dependent rate coefficients for the reaction of Hg with Br and the reaction of Br with Br: A pulsed laser photolysis-pulsed laser induced fluorescence study. *The Journal of Physical Chemistry A*, *110*(21), 6623–6632. https://doi.org/10.1021/jp054688j
Donohoue, D. L., Bauer, D., & Hynes, A. J. (2005). Temperature and pressure dependent rate coefficients for the reaction of Hg with Cl and the reaction of Cl with Cl: A pulsed laser Photolysis−Pulsed laser induced fluorescence study. *The Journal of Physical Chemistry A*, *109*(34), 7732–7741. https://doi.org/10.1021/jp051354l
Eyring, V., Shepherd, T. G., & Waugh, D. W. (Eds.) (2010). *SPARC CCMVal report on the evaluation of chemistry-climate models*, *SPARC report (Vol. 5)*. SPARC Office. Retrieved from http://www.sparc-climate.org/publications/sparc-reports/
Fdez. Galván, I., Vacher, M., Alavi, A., Angeli, C., Aquilante, F., Autschbach, J., et al. (2019). OpenMolcas: From source code to insight. *Journal of Chemical Theory and Computation*, *15*(11), 5925–5964. https://doi.org/10.1021/acs.jctc.9b00532
Fernandez, R. P., Kinnison, D. E., Lamarque, J. F., Tilmes, S., & Saiz-Lopez, A. (2017). Impact of biogenic very short-lived bromine on the Antarctic ozone hole during the 21st century. *Atmospheric Chemistry and Physics*, *17*(3), 1673–1688. https://doi.org/10.5194/acp-17-1673-2017
Fernandez, R. P., Salawitch, R. J., Kinnison, D. E., Lamarque, J.-F., & Saiz-Lopez, A. (2014). Bromine partitioning in the tropical tropopause layer: Implications for stratospheric injection. *Atmospheric Chemistry and Physics*, *14*(24), 13391–13410. https://doi.org/10.5194/acp-14-13391-2014
Finley, J., Malmqvist, P.-Å., Roos, B. O., & Serrano-Andrés, L. (1998). The multi-state CASPT2 method. *Chemical Physics Letters*, *288*(2), 299–306. https://doi.org/10.1016/S0009-2614(98)00252-8
Forsberg, N., & Malmqvist, P.-Å. (1997). Multiconfiguration perturbation theory with imaginary level shift. *Chemical Physics Letters*, *274*(1), 196–204. https://doi.org/10.1016/S0009-2614(97)00669-6
Fuchs, N. A. (1964). *The mechanics of aerosols*. Pergamon Press.

Garcia, R. R., Smith, A. K., Kinnison, D. E., de la Cámara, Á., & Murphy, D. J. (2017). Modification of the gravity wave parameterization in the Whole atmosphere community climate model: Motivation and results. *Journal of the Atmospheric Sciences*, *74*(1), 275–291. https://doi.org/10.1175/JAS-D-16-0104.1

Gelaro, R., McCarty, W., Suárez, M. J., Todling, R., Molod, A., Takacs, L., et al. (2017). The modern-era retrospective analysis for research and applications, version 2 (MERRA-2). *Journal of Climate*, *30*(14), 5419–5454. https://doi.org/10.1175/JCLI-D-16-0758.1

Ghigo, G., Roos, B. O., & Malmqvist, P.-Å. (2004). A modified definition of the zeroth-order Hamiltonian in multiconfigurational perturbation theory (CASPT2). *Chemical Physics Letters*, *396*(1), 142–149. https://doi.org/10.1016/j.cplett.2004.08.032

Gill, E. K., & Laidler, K. J. (1958). Reactions involving electronically-excited oxygen. *Canadian Journal of Chemistry*, *36*(1), 79–88. https://doi.org/10.1139/v58-009

Gomez Martin, J. C., Lewis, T. R., Douglas, K. M., Blitz, M., Saiz-Lopez, A., & Plane, J. M. C. (2022). The reaction between HgBr and O3: Kinetic study and atmospheric implications. *Phys. Chem. Chem. Phys.*, *24*(20), 12419–12432. https://doi.org/10.1039/D2CP00754A

Goodsite, M. E., Plane, J. M. C., & Skov, H. (2004). A theoretical study of the oxidation of Hg-0 to HgBr2 in the troposphere. *Environmental Science and Technology*, *38*(6), 1772–1776. https://doi.org/10.1021/es034680s

Granucci, G., Persico, M., & Toniolo, A. (2001). Direct semiclassical simulation of photochemical processes with semiempirical wave functions. *The Journal of Chemical Physics*, *114*(24), 10608–10615. https://doi.org/10.1063/1.1376633

Granucci, G., Persico, M., & Zoccante, A. (2010). Including quantum decoherence in surface hopping. *The Journal of Chemical Physics*, *133*(13), 134111. https://doi.org/10.1063/1.3489004

Gunning, H. E., & Strausz, O. P. (1963). Isotopic effects and the mechanism of energy transfer in mercury photosensitization. In *Advances in photochemistry* (pp. 209–274). John Wiley & Sons, Ltd. https://doi.org/10.1002/9780470133316.ch7

Iglesias-Suarez, F., Badia, A., Fernandez, R. P., Cuevas, C. A., Kinnison, D. E., Tilmes, S., et al. (2020). Natural halogens buffer tropospheric ozone in a changing climate. *Nature Climate Change*, *10*(2), 147–154. https://doi.org/10.1038/s41558-019-0675-6

Jiao, Y., & Dibble, T. S. (2017). First kinetic study of the atmospherically important reactions $BrHg^{\cdot}$ + NO2 and $BrHg^{\cdot}$ + HOO. *Phys. Chem. Chem. Phys.*, *19*(3), 1826–1838. https://doi.org/10.1039/C6CP06276H

JPL (2011). *Chemical Kinetics and Photochemical Data for Use in Atmospheric Studies* (Vol. 17, pp. 10–16). JPL Publication.

Khiri, D., Louis, F., Černušák, I., & Dibble, T. S. (2020). BrHgO• + CO: Analogue of OH + CO and reduction path for Hg(II) in the atmosphere. *ACS Earth and Space Chemistry*, *4*(10), 1777–1784. https://doi.org/10.1021/acsearthspacechem.0c00171

Lam, K. T., Wilhelmsen, C. J., Schwid, A. C., Jiao, Y., & Dibble, T. S. (2019). Computational study on the photolysis of BrHgONO and the reactions of BrHgO with CH4, C2H6, NO, and NO2: Implications for formation of Hg(II) compounds in the atmosphere. *Journal of Physical Chemistry A*, *123*(8), 1637–1647. research-article. https://doi.org/10.1021/acs.jpca.8b11216

Li, Z., Xiao, Y., & Liu, W. (2014). On the spin separation of algebraic two-component relativistic Hamiltonians: Molecular properties. *The Journal of Chemical Physics*, *141*(5), 54111. https://doi.org/10.1063/1.4891567

Lindqvist, O. L. I. V. E. R., & Rodhe, H. (1985). Atmospheric mercury-a review. *Tellus*, *37B*(3), 136–159. https://doi.org/10.1111/j.1600-0889.1985.tb00062.x

MacDonald, S. M., Gómez Martín, J. C., Chance, R., Warriner, S., Saiz-Lopez, A., Carpenter, L. J., & Plane, J. M. C. (2014). A laboratory characterisation of inorganic iodine emissions from the sea surface: Dependence on oceanic variables and parameterisation for global modelling. *Atmospheric Chemistry and Physics*, *14*(11), 5841–5852. https://doi.org/10.5194/acp-14-5841-2014

Mai, S., Marquetand, P., & González, L. (2015). A general method to describe intersystem crossing dynamics in trajectory surface hopping. *International Journal of Quantum Chemistry*, *115*(18), 1215–1231. https://doi.org/10.1002/qua.24891

Mai, S., Marquetand, P., & González, L. (2018). Nonadiabatic dynamics: The SHARC approach. *WIREs Computational Molecular Science*, *8*(6), e1370. https://doi.org/10.1002/wcms.1370

Mai, S., Müller, T., Plasser, F., Marquetand, P., Lischka, H., & González, L. (2014). Perturbational treatment of spin-orbit coupling for generally applicable high-level multi-reference methods. *The Journal of Chemical Physics*, *141*(7), 74105. https://doi.org/10.1063/1.4892060

Mai, S., Richter, M., Heindl, M., Menger, M. F. S. J., Atkins, A., Ruckenbauer, M., et al. (2019). *SHARC2.1: Surface hopping including arbitrary couplings – program package for non-adiabatic dynamics*. Sharc-Md.Org.

Malmqvist, P.-Å., & Roos, B. O. (1989). The CASSCF state interaction method. *Chemical Physics Letters*, *155*(2), 189–194. https://doi.org/10.1016/0009-2614(89)85347-3

Morand, J.-P., & Nief, G. (1968). Oxydation isotopique du mercure par l'oxygène moléculaire sous l'influence de la radiation 2 357 \AA. *J. Chim. Phys.*, *65*, 2058–2068. https://doi.org/10.1051/jcp/1968652058

Ordóñez, C., Lamarque, J.-F., Tilmes, S., Kinnison, D. E., Atlas, E. L., Blake, D. R., et al. (2012). Bromine and iodine chemistry in a global chemistry-climate model: Description and evaluation of very short-lived oceanic sources. *Atmos. Chem. Phys.*, *12*(3), 1423–1447. https://doi.org/10.5194/acp-12-1423-2012

Pal, B., & Ariya, P. A. (2004). Gas-phase HO•-initiated reactions of elemental mercury: Kinetics, product studies, and atmospheric implications. *Environmental Science and Technology*, *38*(21), 5555–5566. https://doi.org/10.1021/es0494353

Peng, D., & Reiher, M. (2012). Exact decoupling of the relativistic Fock operator. *Theoretical Chemistry Accounts*, *131*(1), 1081. https://doi.org/10.1007/s00214-011-1081-y

Peterson, K. A., Figgen, D., Goll, E., Stoll, H., & Dolg, M. (2003). Systematically convergent basis sets with relativistic pseudopotentials. II. Small-core pseudopotentials and correlation consistent basis sets for the post-d group 16–18 elements. *The Journal of Chemical Physics*, *119*(21), 11113–11123. https://doi.org/10.1063/1.1622924

Plasser, F., Granucci, G., Pittner, J., Barbatti, M., Persico, M., & Lischka, H. (2012). Surface hopping dynamics using a locally diabatic formalism: Charge transfer in the ethylene dimer cation and excited state dynamics in the 2-pyridone dimer. *The Journal of Chemical Physics*, *137*(22), 22A514. https://doi.org/10.1063/1.4738960

Prados-Roman, C., Cuevas, C. A., Fernandez, R. P., Kinnison, D. E., Lamarque, J.-F., & Saiz-Lopez, A. (2015). A negative feedback between anthropogenic ozone pollution and enhanced ocean emissions of iodine. *Atmospheric Chemistry and Physics*, *15*(4), 2215–2224. https://doi.org/10.5194/acp-15-2215-2015

Reiher, M., & Wolf, A. (2004a). Exact decoupling of the Dirac Hamiltonian. I. General theory. *The Journal of Chemical Physics*, *121*(5), 2037–2047. https://doi.org/10.1063/1.1768160

Reiher, M., & Wolf, A. (2004b). Exact decoupling of the Dirac Hamiltonian. II. The generalized Douglas–Kroll–Hess transformation up to arbitrary order. *The Journal of Chemical Physics*, *121*(22), 10945–10956. https://doi.org/10.1063/1.1818681

Richter, M., Marquetand, P., González-Vázquez, J., Sola, I., & González, L. (2011). SHARC: Ab initio molecular dynamics with surface hopping in the adiabatic representation including arbitrary couplings. *Journal of Chemical Theory and Computation*, *7*(5), 1253–1258. https://doi.org/10.1021/ct1007394

Rienecker, M. M., Suarez, M. J., Gelaro, R., Todling, R., Bacmeister, J., Liu, E., et al. (2011). MERRA: NASA's modern-era retrospective analysis for research and applications. *Journal of Climate*, *24*(14), 3624–3648. https://doi.org/10.1175/JCLI-D-11-00015.1

Roos, B. O., Lindh, R., Malmqvist, P.-Å., Veryazov, V., & Widmark, P.-O. (2005). New relativistic ANO basis sets for transition metal atoms. *The Journal of Physical Chemistry A*, *109*(29), 6575–6579. https://doi.org/10.1021/jp0581126

Roos, B. O., Taylor, P. R., & Sigbahn, P. E. M. (1980). A complete active space SCF method (CASSCF) using a density matrix formulated super-CI approach. *Chemical Physics*, *48*(2), 157–173. https://doi.org/10.1016/0301-0104(80)80045-0

Saiz-Lopez, A., Fernandez, R. P., Ordóñez, C., Kinnison, D. E., Gómez Martín, J. C., Lamarque, J.-F., & Tilmes, S. (2014). Iodine chemistry in the troposphere and its effect on ozone. *Atmos. Chem. Phys.*, *14*(23), 13119–13143. https://doi.org/10.5194/acp-14-13119-2014

Saiz-Lopez, A., Travnikov, O., Sonke, J. E., Thackray, C. P., Jacob, D. J., Carmona-García, J., et al. (2020). Photochemistry of oxidized Hg(I) and Hg(II) species suggests missing mercury oxidation in the troposphere. *Proceedings of the National Academy of Sciences*, *117*(49), 30956–30949. LP – 30956. https://doi.org/10.1073/pnas.1922486117

Sitkiewicz, S. P., Oliva, J. M., Dávalos, J. Z., Notario, R., Saiz–Lopez, A., Alcoba, D. R., et al. (2016). Ab initio quantum–chemical computations of the electronic states in HgBr2 and IBr: Molecules of interest on the Earth's atmosphere. *The Journal of Chemical Physics*, *145*(24), 244304. https://doi.org/10.1063/1.4971856

Solomon, S., Kinnison, D., Bandoro, J., & Garcia, R. (2015). Simulation of polar ozone depletion: An update. *Journal of Geophysical Research: Atmospheres*, *120*(15), 7958–7974. https://doi.org/10.1002/2015JD023365

Vallet, V., Maron, L., Teichteil, C., & Flament, J.-P. (2000). A two-step uncontracted determinantal effective Hamiltonian-based SO–CI method. *The Journal of Chemical Physics*, *113*(4), 1391–1402. https://doi.org/10.1063/1.481929

Verlet, L. (1967). Computer "experiments" on classical fluids. I. Thermodynamical properties of Lennard-Jones molecules. *Phys. Rev.*, *159*(1), 98–103. https://doi.org/10.1103/PhysRev.159.98

Wang, F., & Ziegler, T. (2005). A simplified relativistic time-dependent density-functional theory formalism for the calculations of excitation energies including spin-orbit coupling effect. *The Journal of Chemical Physics*, *123*(15), 154102. https://doi.org/10.1063/1.2061187

Weigend, F., & Ahlrichs, R. (2005). Balanced basis sets of split valence{, } triple zeta valence and quadruple zeta valence quality for H to Rn: Design and assessment of accuracy. *Phys. Chem. Chem. Phys.*, *7*(18), 3297–3305. https://doi.org/10.1039/B508541A

Wigner, E. (1932). On the quantum correction for thermodynamic equilibrium. *Phys. Rev.*, *40*(5), 749–759. https://doi.org/10.1103/PhysRev.40.749